Case Studies in Construction Materials 17 (2022) e01428

Contents lists available at ScienceDirect

Case Studies in Construction Materials

journal homepage: www.elsevier.com/locate/cscm

Case study

Metakaolin/sludge based geopolymer adsorbent on high removal efficiency of Cu^{2+}

Pilomeena Arokiasamy [a,b], Mohd Mustafa Al Bakri Abdullah [a,b,*], Shayfull Zamree Abd Rahim [a,c], Mohd Remy Rozainy Mohd Arif Zainol [d], Mohd Arif Anuar Mohd Salleh [a,c], Marwan Kheimi [e], Jitrin Chaiprapa [f], Andrei Victor Sandu [g], Petrica Vizureanu [g], Rafiza Abdul Razak [a], Noorina Hidayu Jamil [c]

[a] Centre of Excellence Geopolymer & Green Technology (CEGeoGTech), Universiti Malaysia Perlis (UniMAP), Perlis 02600, Malaysia
[b] Faculty of Chemical Engineering Technology, Universiti Malaysia Perlis (UniMAP), Perlis 02600, Malaysia
[c] Faculty of Mechanical Engineering Technology, Universiti Malaysia Perlis (UniMAP), Perlis 02600, Malaysia
[d] River Engineering and Urban Drainage Research Centre (REDAC), Universiti Sains Malaysia, Penang 14300, Malaysia
[e] Department of Civil Engineering, Faculty of Engineering-Rabigh Branch, King Abdulaziz University, Jeddah 21589, Saudi Arabia
[f] Synchrotron Light Research Institute, Muang, Nakhon Ratchasima 30000, Thailand
[g] Faculty of Material Science and Engineering, Gheorghe Asachi Technical University of Iasi, 41 D. Mangeron St., Iasi 700050, Romania

ARTICLE INFO

Keywords:
Geopolymer
Metakaolin
Sludge
Adsorbent
Adsorption

ABSTRACT

Activated carbon (AC) has received a lot of interest from researchers for the removal of heavy metals from wastewater due to its abundant porous structure. However, it was found unable to meet the required adsorption capacity due to its amorphous structure which restricts the fundamental studies and structural optimization for improved removal performance. In addition, AC is not applicable in large scale wastewater treatment due its expensive synthesis and difficulty in regeneration. Thus, the researchers are paying more attention in synthesis of low cost geopolymer based adsorbent for heavy metal removal due its excellent immobilization effect. However, limited studies have focused on the synthesis of geopolymer based adsorbent for heavy metal adsorption by utilizing industrial sludge. Thus, the aim of this research was to develop metakaolin (MK) based geopolymer adsorbent with incorporation of two types of industrial sludge (S1 and S3) that could be employed as an adsorbent for removing copper (Cu^{2+}) from aqueous solution through the adsorption process. The effects of varied solid to liquid ratio (S/L) on the synthesis of metakaolin/sludge based geopolymer adsorbent and the removal efficiency of Cu^{2+} by the synthesis adsorbent were studied. The raw materials and synthesized geopolymer were characterized by using x-ray fluorescence (XRF), x-ray diffraction (XRD), scanning electron microscope (SEM), fourier transform infrared spectroscopy (FTIR), Brunauer-Emmett-Teller (BET) and micro XRF. The concentration of Cu^{2+} before and after adsorption was determined by atomic absorption spectroscopy (AAS) and the removal efficiency was calculated. The experimental data indicated that the synthesized geopolymer at low S/L ratio has achieved the highest removal efficiency of Cu^{2+} about 99.62 % and 99.37 % at 25 %:75 % of MK/S1 and 25 %:75 % of MK/S3 respectively compared to pure MK based geopolymer with 98.56 %. The best S/

* Corresponding author at: Centre of Excellence Geopolymer & Green Technology (CEGeoGTech), Universiti Malaysia Perlis (UniMAP), Perlis 02600, Malaysia.
E-mail address: mustafa_albakri@unimap.edu.my (M.M.A.B. Abdullah).

https://doi.org/10.1016/j.cscm.2022.e01428
Received 13 July 2022; Received in revised form 19 August 2022; Accepted 22 August 2022
Available online 24 August 2022

L ratio for MK/S1 and MK/S3 is 0.6 at which the reaction between the alkaline activator and the aluminosilicate materials has improved and enhanced the geopolymerization process. Finally, this work clearly indicated that industrial sludge can be utilized in developing low-cost adsorbent with high removal efficiency.

1. Introduction

Heavy metals are widely used in the engineering, papermaking, fine chemicals, dyes, paints, pharmaceuticals, petrochemical, and textile sectors, resulting in significant concentrations of heavy metal ions in their effluent. Heavy metals are specified as elements with atomic weight ranging from 63.5 g/mol to 200.6 g/mol with a specific density more than 5.0 g/cm^3 [1–3]. According to United States Environmental Protection Agency, the most toxic heavy metal includes arsenic (As), copper (Cu), mercury (Hg), nickel (Ni), cadmium (Cd), lead (Pb) and chromium (Cr) [3,4]. These heavy metal ions have carcinogenic, teratogenic, mutagenic, non-biodegradable, and bioaccumulative properties, posing a serious hazard to the environment and human health. Therefore, these heavy metal ions need to be removed from the wastewater prior to being disposed into the ecosystem. There have been numerous methods for eliminating heavy metals from wastewater in the past [5–7].

Chemical precipitation, ion exchange, electrocoagulation, membrane filtration and adsorption methods can be used to remove heavy metals from wastewater [5–7]. Among other heavy metal treatment methods, adsorption has received a lot of attention because of its ease of use, minimum secondary contamination, high cost-effectiveness, and low energy consumption in removing heavy metals quickly from aqueous solution. The adsorbent is the most important component of the adsorption process. Activated carbon (AC), biochar, carbon nanotube (CNT), zeolite, geopolymer and clay mineral are some of the well-known adsorbents [8–10].

Among these adsorbents, AC is a carbonaceous material with high surface area and amorphous nature and offers a wider range of uses in water remediation process [11]. AC can be synthesized from carbon-rich organic materials including coconut shells, wood, coal, peat, and other sources. AC is frequently employed in wastewater treatment due to its extensive porous structure and large surface area. [12]. However, it failed to attain the specified adsorption capacity for heavy metal removal [13]. This is because, the disordered structure of amorphous carbon restricts the fundamental studies and structural optimization for improved removal performance [14]. Besides, its use in large-scale wastewater treatment is restricted by the expensive synthesis and challenging regeneration.

Hence, geopolymer has gained great interest among researchers for the development of cost-effective adsorbents as it has excellent adsorption properties when compared to other adsorbents. Geopolymer composed of three-dimensional (3D) network structure, with fixed-sized pores and paths that allow only certain heavy metals to pass through. Geopolymer is composed of a polymeric silicon-oxygen-aluminum (Si-O-Al) framework with alternating linked silicon (SiO_4) and aluminum (AlO_4) tetrahedral by sharing all bridged oxygen atoms [15,16]. Geopolymers are semi-crystalline to amorphous structures and are made by an exothermal chemical reaction in an alkaline medium between silica and alumina-rich precursors and alkaline activators at low temperature [16,17]. Negatively charged alumina-silicate framework of geopolymer makes them a useful adsorbent to treat contaminated water at which it offers ion exchangeability between cations in alkaline activator and heavy metal ions. In addition, geopolymers are made up of cyclic molecular chains composed of a "crystal-like" structure [18,19]. Closed cage-like cavity generated through the conjunction of ring molecules can aid in the removal of heavy metals or other pollutants by fixing it in the cavity. Geopolymer materials are regarded as environmentally friendly owing to their low manufacturing temperature, low energy usage, and low carbon dioxide emissions. Moreover, geopolymers have remarkable advantages such as low cost, facile synthesis and local avail-ability of raw materials [18,20]. However, decreased of workability and high heat of hydration released are related to the disadvantages of geopolymer. In comparison to cementitious material, geopolymer produced by alkali activation releases more heat which will results in loss of water [21–23]. The continual loss of water from the matrix can result in inadequate wetting of the precursor particles, which would significantly impact

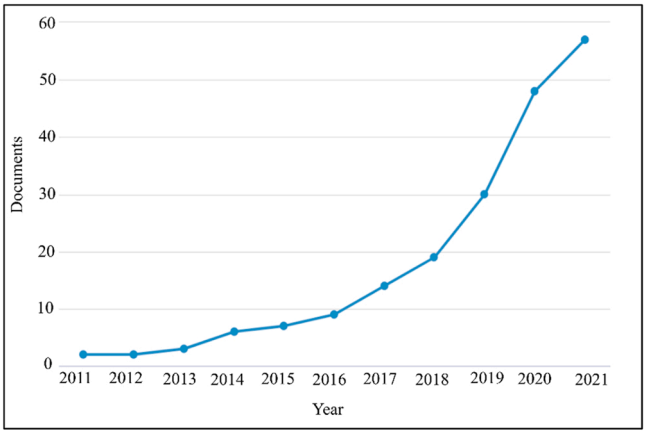

Fig. 1. Documents published on geopolymer adsorbents.

the workability of paste and make molding very challenging. The line graph in Fig. 1 shows the number of documents published on geopolymer adsorbents in a span of ten years. The increasing trend of documents published over the years, indicates that most of the researchers have been focusing on investigating geopolymer adsorbents towards heavy metal removal from wastewater. Geopolymers are formed from various geological origins like kaolin and metakaolin as well as industrial waste such as red mud, fly ash, slag, and sludge. In 2019, Darmayanti et al. [24] investigated the adsorption of Cu^{2+} by fly ash based geopolymer. Moreover, a study by Panda et al. [25] explored the effectiveness of geopolymer adsorbent synthesized from pyrophyllite mine waste towards adsorption of Co^{2+}, Cd^{2+}, Ni^{2+}, and Pb^{2+} from aqueous solution.

On the other hand, sludge as a raw material, does contain some significant components compared to other industrial wastes. The primary inorganic components of sludge are SiO_2, Fe_2O_3, and Al_2O_3, which make it potentially useful as a renewable energy source. In addition, sludge contains high concentrations of inorganic salts including inorganic ions such as (CO_3^{2-}, PO_4^{3-}, SO_4^{2-} and NO^{3-}) and other elements such as (Si, Al, K, Na, Ca and Mg) [26,27]. Thus, it can effectively adsorb heavy metal ions by the combined contribution of ion exchange, precipitation and ion complexation with heavy metals. In addition, the presence of metal oxides and inorganic salts in sludge will increase the active sites on the surface of geopolymer. Water treatment sludge (WTS) is a heterogeneous solid waste which is high in Si and Al and closely resembles natural aluminosilicates [28]. Formation of residue in the water treatment process by the addition of chemical reagents in the removal of fine particles and organic substances dissolution is called WTS, while waste glass sludge (WGS) is a byproduct of the numerous glass industries where the glass materials are cut and polished for manufacturing processes. WGS has greater amount of SiO_2 and it has extremely small particles [29]. However, limited studies focused on the synthesis of geopolymer based adsorbent for heavy metal adsorption by utilizing sludge. Thus, the aim of this study is to develop metakaolin (MK) based geopolymer adsorbents by incorporating two types of industrial sludges (S1 and S3) and also to investigate the impact of various solid to liquid ratios (S/L) on the geopolymerization process and also on the removal efficiency of Cu^{2+}.

2. Materials and methods

2.1. Raw materials

In this study, Kaolin (K), industrial sludge (S1) and industrial sludge (S3) were used as raw materials. Kaolin was supplied by Associated Kaolin Industries Sdn Bhd, Petaling Jaya, Selangor, Malaysia, while S1 and S3 were supplied by Alam Aliran Kualiti (M) Sdn Bhd, Bukit Mertajam, Penang, Malaysia. Calcined kaolin was used as the starting material and S1 or S3 as a filler in the geopolymerization process. Sodium hydroxide (NaOH) and sodium silicate ($NaSiO_3$) were used to make alkaline activator. NaOH and $NaSiO_3$ were provided by Formosa Plastic Corporation, Taiwan and South Pacific Chemical Industries Sdn Bhd, Perai, Penang, Malaysia respectively.

2.2. Preparation of geopolymer adsorbent

Synthesis of geopolymer adsorbent involves several steps. First, S1 and S3 are oven dried at 100 ºC for 24 h to remove the moisture content. Then, Kaolin is calcined at 750 ºC for 5 h to increase the reactivity [30,31]. According to Oualit et al. [32], the first stage of the decomposition of kaolin begins at about 80 ºC to 150 ºC caused by the loss of moisture from kaolin. At the second stage, the highest mass loss occurs at temperatures between 400 ºC and 700 ºC, which is linked to the loss of water from kaolinite (dehydroxylation) and the creation of the metakaolinite phase. At temperatures between 650 ºC and 750 ºC, kaolinite is completely transformed into metakaolin. During calcination, the structural water is gradually lost, the aluminum coordination changes from six to four, and the structure becomes amorphous. After that, the raw materials are sieved through 300 μm to obtain fine particles. At the first stage, MK was mixed with S1 or S3 to prepare solid precursors at varied ratios of MK/S1 and MK/S3 as shown in Table 1. The ratio of MK to S1 or S3 was chosen to partially replace the aluminosilicate source which is MK, by using sludge with the increment of 25 total weight %. The alkaline activator ratio (Na_2SiO_3/NaOH) determines the modulus ratio of SiO_2/Na_2O which is the essential parameter in the formation of geopolymer product. At high alkali activator ratio, increasing the modulus ratio of SiO_2/Na_2O results in more Si ions in the solution, which can improve the polymerization and yield more compact silicon-rich gel phase [34,35]. Thus, alkaline activator as liquid part was prepared using 10 M of NaOH and Na_2SiO_3 with modulus ratio of Na_2SiO_3:NaOH being 1.5 [25,33]. Thereafter, the raw materials were mixed with alkaline activator at different solid-to-liquid (S:L) ratios by using mechanical mixer for 15 mins [36] as shown in Fig. 2. The varied S:L ratio was chosen based on the workability of pure MK based geopolymer paste at S:L ratio of 1:0. As the workability of pure MK geopolymer paste is lowest at S:L ratio of 1:0, thus, the ratio below 1:0 is considered for the geopolymerization process. Then, the obtained paste was oven cured at constant temperature for 2 days. Excessive alkaline residue in geopolymer will

Table 1
Parameters of synthesis geopolymer adsorbents.

Parameter	Details
MK: S1	100:0, 75:25, 50:50, 25:75
MK: S3	100:0, 75:25, 50:50, 25:75
$NaSiO_3$: NaOH	1.5
S: L	0.4, 0.6, 0.8, 1.0
Curing temperature	60 ºC

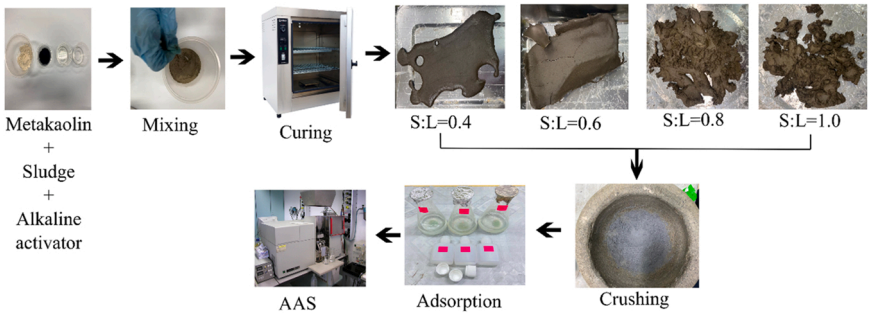

Fig. 2. Synthesis of metakaolin/sludge geopolymer adsorbent.

increase the pH of an aqueous solution containing heavy metals, and encourage the hydroxide precipitation process, consequently reducing the effectiveness of adsorption [37]. Therefore, the hardened geopolymer paste was then crushed by using porcelain mortar and washed three times using distilled water until the pH of the wash water is maintained at 7.0 ± 0.5 for at least 24 h. After that, the washed and dried powder was sieved to obtain a particle diameter of < 300 μm, which is then used for the sorption process.

In the second stage, stock solution (1000 mg/L) of Cu^{2+} was prepared by dissolving an appropriate amount of analytical grade reagents copper sulfate pentahydrate ($CuSO_40.5H_2O$) in distilled water and then it was diluted to prepare 100 mg/L of initial copper solution. The pH of the solution was adjusted using 0.01 HCl or 0.01 NaOH. For batch adsorption experiment, a constant amount of geopolymer adsorbent was mixed with 100 ml of prepared copper solution and shaken for 1 h at 220 rpm as described in Table 2. The formulated products were labelled GMK100–0.4, GMK100–0.6, GMK100–0.8 and GMK100–1.0, where 0.4, 0.6, 0.8 and 1.0 represent S/L ratios, MK100 represents the percentage of MK by weight and G represents geopolymerization process as tabulated in Table 3. The experiment was repeated under same experiment conditions for MK: S1 and MK: S3 at 75:25, 50:50, and 25:75. Finally, the adsorption efficiency of geopolymer adsorbent was compared to the reference sample which was prepared without the geopolymerization process.

2.3. Testing

The chemical composition of raw materials was determined by X-ray fluorescence (XRF) and the phases present were characterized by a diffractometer-XRD system (model Bruker D2 Phaser), using Cu-Kα (at wavelength 1.54184 [A]) radiation, fitted with a Cu tube on the secondary optics, and operated under 30 kV power and 10 mA current. The scanning 2θ ranged between 5 ° to 90 °. Highscore Plus software was used to conduct the semiqualitative analysis of the XRD data in order to identify the amorphous structure and crystalline phases of raw materials and geopolymer adsorbents.

Fourier-transform infrared spectroscopy (FTIR) analysis was conducted using PerkinElmer (Frontier) to record transmittance spectra in the 400–4000 cm− 1 region, with a resolution of 4 cm^{-1} (8 scans) to analyze the functional groups of raw materials and synthesized geopolymer adsorbents. 2 mg of sample powder mixed with 198 mg of potassium bromide (KBr) was then compacted into disc under a pressure of 8 tons for 2 mins using a hydraulic press.

The microstructure and surface elemental distribution of raw materials and geopolymer adsorbents before and after adsorption was observed using a Scanning electron microscope (SEM) JEOL JSM-6460LA combined with an energy-dispersive detector at an acceleration energy of 15 keV. Sputter-coater Q150R S was used to coat the material by a conductive material which is gold for 1 min to avoid charging of electrons during examination in SEM.

Brunauer-Emmett-Teller (BET) surface area and pore size distribution of raw materials were studied on Micromeritics Tristar II by degassing the sample with nitrogen gas at 200 ºC for 6 h.

After adsorption, the supernatant liquid of the reaction was filtered and separated. The changes in the Cu^{2+} concentration was determined by conducting atomic absorption spectroscopy (AAS) (model Perkin Elmer Analyst 800). The obtained results were used to calculate the removal efficiency of Cu^{2+} by synthesized geopolymer adsorbents by using the formula shown in Eq. (1).

$$Removal\quad efficiency: \quad \frac{(Initial\quad concentration - Final\quad concentration)}{Initial\quad concentration} x\quad 100 \tag{1}$$

Synchrotron micro-X-ray fluorescence at BL 7.2 W:MX beamline was used to determine the distributions of elements in synthesized geopolymer adsorbents which are located at the Synchrotron Light Research Institute (SLRI), Thailand. Synchrotron micro-XRF is an

Table 2
Parameters of adsorption experiment.

Parameter	Details
Adsorbent dosage	0.15 g
pH	5
Temperature	25 ºC
Time	1 h

Table 3
Sample descriptions according to process.

Process	Sample	Process	Sample	S/L ratio
Without geopolymerization	MK	With geopolymerization (G)	GMK100	0.4,0.6,0.8,1.0
	S1		GMK75S1	0.4,0.6,0.8,1.0
	S3		GMK75S3	0.4,0.6,0.8,1.0
	MK75S1		GMK50S1	0.4,0.6,0.8,1.0
	MK75S3		GMK50S3	0.4,0.6,0.8,1.0
	MK50S1		GMK25S1	0.4,0.6,0.8,1.0
	MK50S3		GMK25S3	0.4,0.6,0.8,1.0
	MK25S1			
	MK25S3			

advanced technique for non-destructively visualizing the elemental distribution within a sample. The energy of the micro-X-ray beam is fixed at 12 keV. A total spot of 441 with detector time close to 15 % was scanned. The data was analyzed by using PyMca software and the rescaled images of the elemental mapping was illustrated using MATLAB software.

3. Results and discussions

3.1. Characterization of raw materials

The chemical composition of raw materials is tabulated in Table 4. XRF analysis indicates that K is mainly made up of SiO_2, Al_2O_3, with K_2O and Fe_2O_3 as impurities. Upon calcination of K, the data obtained is not much different from kaolin and metakaolin, but the percentage of SiO_2 decreased from 48.85 % to 42.68 %, while Al_2O_3 increased from 43.17 % to 52.96 %. MK can be used in the geopolymerization process as it is rich in Si and Al elements, as the main structural framework of geopolymer consists of Si and Al. In addition, S1 has the highest percentage of SiO_2 (91.64 %) among other elements compared to other raw materials. On the other hand, SiO_2, Al_2O_3, CaO, MgO and Fe_2O_3 are the main components in S3 with total sum-up of 86.98 %. Thus, S1 might have been obtained from glass industry and S3 might have come from water treatment plant based on the chemical composition.

Similar observation was obtained in research conducted by Ayeni et al. [38] at which thermal treatment of K to MK results in an increase in the Al_2O_3 content. In another study by Karatas et al. [39], calcination of kaolin at 600 °C for 3 h caused a decrease in SiO_2 from 73.4 % to 62.34 % and an increase in Al_2O_3 from 18.5 % to 34.68 %. As a result, it was concluded that, calcination favored aluminum availability during geopolymerization contributed to the quick hardening of the geopolymer specimens prepared [28]. Meanwhile, greater amount of Na_2O and MgO in S1 could result in better ion exchangeability with Cu^{2+} and could increase the removal efficiency of Cu^{2+}. In addition, Na is an important element for the geopolymerization process. However, in the case of high Na concentrated geopolymer, excess alkaline residue can be removed by washing with distilled water. Besides, S3 contains greater content of Fe_2O_3 compared to MK and S1. Based on a previous study, the participation of ferric ion in the tetrahedral network of the geopolymer is possible [40]. However, during geopolymerization, reactive iron is anticipated to precipitate quickly in the form of hydroxide or oxyhydroxide phases, eliminating OH ions from the solution and delaying the dissolution of the remaining raw materials. Apart from that, the Si/Al ratio is a critical factor in geopolymerization as it determines the degree of polycondensation, pore development and also directly influences the microstructure of geopolymer. Impurities phases such as Fe, Ti and Ca can influence the Si/Al ratio of geopolymer framework and the geopolymerization process to some extent [41].

The mineral composition of raw materials determined XRD are shown in Fig. 3. K contains kaolinite as main phase with muscovite and quartz as minor phases. After calcination at 750 °C, kaolin is completely transformed into metakaolin with quartz as major phase and muscovite as minor phase. The broad hump in the XRD pattern of MK between 18° and 38° is attributed to amorphous structure of MK. In addition to quartz, MK is mainly hypocrystalline and amorphous. In contrast, the broad band in the XRD pattern of S1 and S3 shows an amorphous structure of sludge materials. While, an amorphous halo with a high loss on ignition is visible, indicating the presence of organic chemicals in the S1 and S3 that volatilize, releasing principally CO, CO_2 and CH_4 [42]. It is also shown in the

Table 4
Chemical composition of raw materials.

Chemical composition	K wt (%)	MK wt (%)	S1 wt (%)	S3 wt (%)
SiO_2	48.85	42.68	91.64	20.09
Al_2O_3	43.17	52.96	0.01	31.50
Na_2O	0.17	0.49	2.75	1.07
MgO	0.41	–	3.80	4.76
CaO	0.20	0.01	0.10	11.97
K_2O	3.53	1.95	0.16	1.21
TiO_2	0.78	0.44	0.02	0.81
Fe_2O_3	2.31	1.28	1.20	18.66
P_2O_5	–	–	0.07	0.21
SO_2	0.22	0.02	0.21	0.29
LOI	0.36	2.12	0.04	9.43

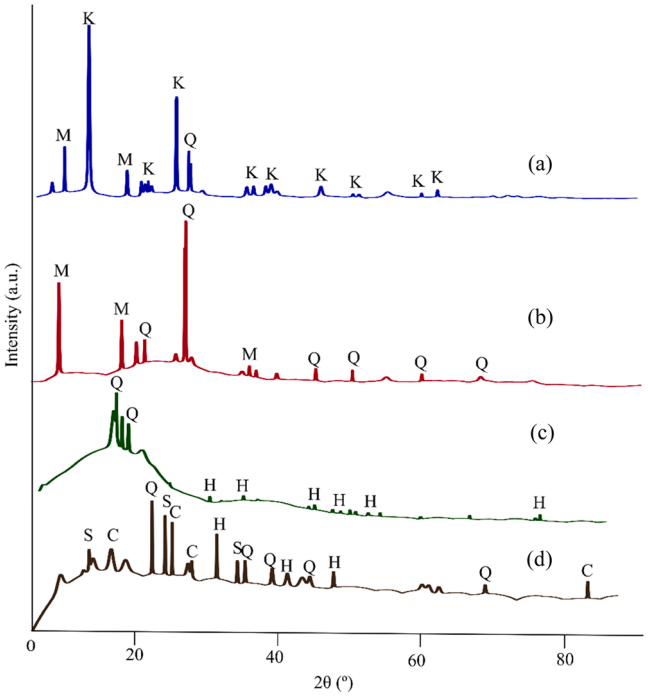

Fig. 3. XRD patterns of (a) K, (b) MK, (c) S1 and (d) S3 (K-kaolinite $Al_2Si_2O_5(OH)_4$, Q-quartz SiO_2, M-muscovite ($KAl_2(AlSi_3O_{10})(OH)$), H-hematite Fe_2O_3, C-calcite ($CaCO_3$), S-sillimanite (Al_2SiO_5).

pattern with the presence of quartz (SiO_2), hematite (Fe_2O_3), calcite ($CaCO_3$) and sillimanite (Al_2SiO_5). S1 is mainly composed of crystalline phases of quartz and hematite while crystalline phases in S3 are quartz, hematite, sillimanite and calcite. The major phase of quartz in S1 is due the presence of high silica content. The existence of calcite and hematite in S3 represents a greater amount of calcium and iron in the XRF results obtained.

The disappearance of peak corresponding to kaolinite is noticed in metakaolin which is explained by the dehydroxylation of the water molecules that occur in the kaolinite structure in metakaolin and indicates the complete transformation of K to MK [43]. Besides, the results obtained also indicate that the material had good calcination and almost all of the kaolinite has been calcined. However, the presence of the quartz phase, which did not undergo amorphization completely after heat treatment, demonstrated that the K utilized in the calcination was not pure kaolinite [44]. The broad hump of S1 and S3 represents high concentration of disordered and unstable structures. This is because, the bonding in amorphous has short range order and is irregularly created when atomic locations are not randomly dispersed in 3-D orientation and thus amorphous is commonly formed in instable phase. Thus, the reactivity of materials

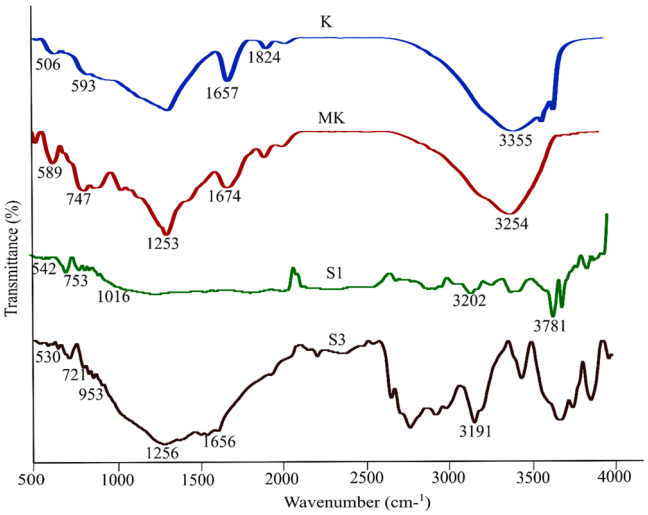

Fig. 4. FTIR spectrum of raw materials.

increased when it is in amorphous phase and geopolymerization process is enhanced.

FTIR spectra of K, MK, S1 and S3 are illustrated in Fig. 4. The peak of kaolin corresponding to 3355 cm^{-1} is related to stretching of OH groups [45]. The ordered structure of kaolinite is confirmed by the well-defined peak in this area, while a peak at 1657 cm^{-1} is related to deformation of the hydroxyl group and a strong peak uptake of 1824 cm^{-1} is due to absorption of -OH buckling vibrations trapped in the crystal lattice [46]. In addition, absorption bands at 593 cm^{-1} and 427 cm^{-1} are due to bending vibration of Si-O-Al and Si-O-Si respectively [47]. Upon calcination of kaolin, the peaks related to stretching and deformation of OH^- can still be observed in the FTIR spectra of MK with a new peak corresponding to bending vibration of Si-O-Al at 747 cm^{-1}. The stretching vibration of Al (VI)–O are connected to 747 cm^{-1} in the IR spectra of MK which will reduce after geopolymerization during hydration reaction [48]. Moreover, FTIR spectra of S1 and S3 indicate the presence of OH, Si-O-Al and Si-O-Si functional groups. Absorption frequency of peak at 3202 cm^{-1}, 3191 cm^{-1} and 1656 cm^{-1} are related to OH functional groups, while 1016 cm^{-1} and 953 cm^{-1} corresponded to stretching vibration of Si-O-T (T = Si or Al). Besides, the FTIR spectrum at 753 cm^{-1} and 721 cm^{-1} and 542 cm^{-1} and 530 cm^{-1} indicate the bending vibrations of Si-O-Al and Si-O-Si respectively.

Fig. 5 shows the microstructure of raw materials. The layered structure of K is shown in Fig. 5(a). However, upon calcination, the amount of coarse fraction increased as revealed in Fig. 5(b). Calcination appears to have affected the crystalline arrangement of kaolinite. The disordered phase is indicated by the uneven arrangement and broken edges of the kaolinite platelets. On the other hand, Fig. 5(c) reveals that the material is made up of a large number of spheres like particles stacked on top of each other. This indicates that there are numerous pore channels between and within particles, indicating that small molecules have an easier time penetrating the material's interior structure. In contrast, S3 particles consist of flake-like structure as shown in Fig. 5(d).

The nitrogen adsorption and desorption isotherm of the MK, S1 and S3 used in this study is shown in Fig. 6. The adsorption and desorption isotherm curve of MK and S3 is almost shown the similar trend. The isothermal adsorption of these samples referred to as IV type at which indicating the mesopores structure of the materials [49]. However, S1 is obtained at a completely different trend compared to MK and S3 at which the amount of adsorbed nitrogen is reduced with increasing relative pressure. This observation demonstrates the small surface area and pore volume of S1 material compared to MK and S3. The surface area and pore characteristics of MK, S1 and S3 are tabulated in Table 5. The BET specific surface area of MK is approximately 8.38 m^2/g which is larger than S1 and S3 with the pore volume of MK and S3 obtained having the same value at 0.02 cm^3/g. The surface area of MK used in this study is larger than MK (2.54 m^2/g) used in research by Lan et al. [25]. However, the average pore size of S3 is higher than MK and S1.

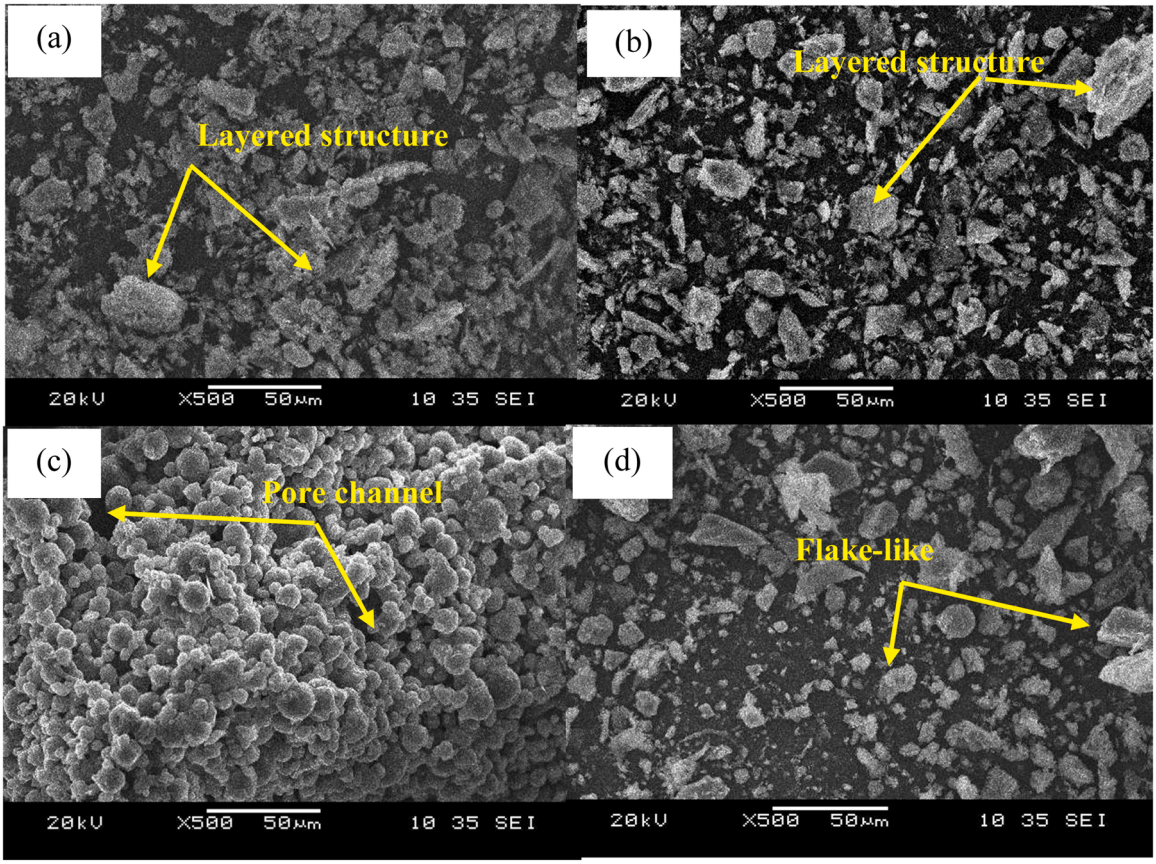

Fig. 5. Morphology of raw materials (a) kaolin, (b) metakaolin, (c) S1, (d) S3.

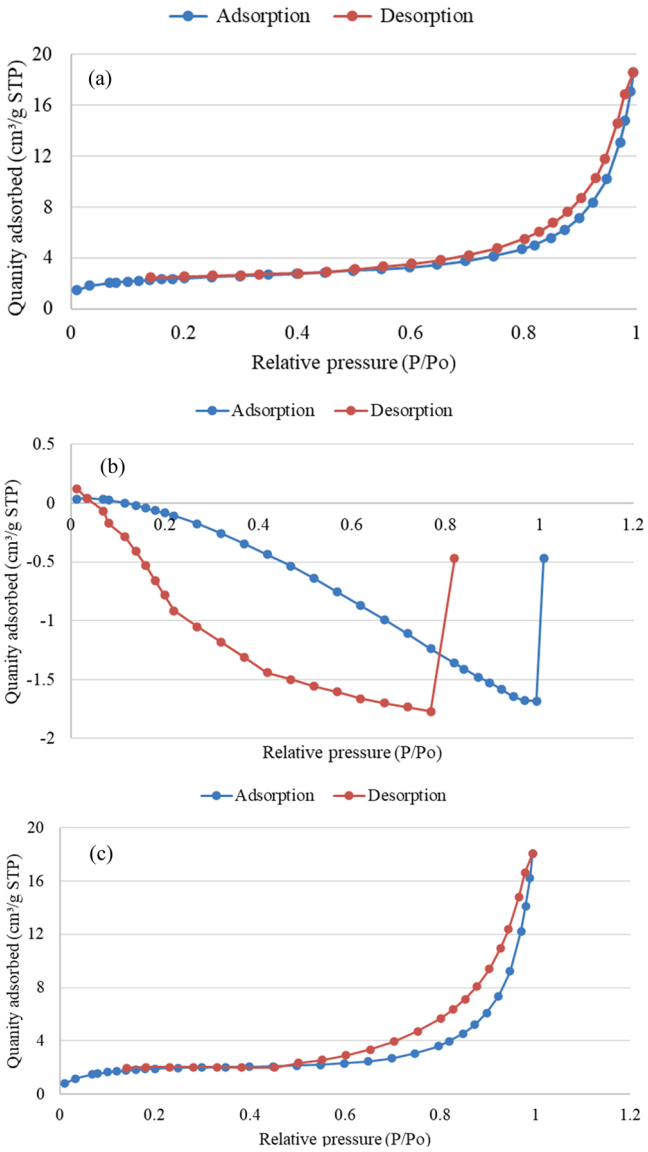

Fig. 6. Nitrogen adsorption and desorption isotherm of raw materials: (a) MK, (b) S1 and (c) S3.

Table 5
BET surface area, pore volume and average pore size of samples.

Sample	S_{BET} (m^2/g)	Pore volume (cm^3/g)	Average pore size (nm)
MK	8.38	0.02	96.70
S1	0.04	–	–
S3	6.98	0.02	108.43

3.2. Characterization of synthesized geopolymer adsorbent

The phases present in the sample of synthesized geopolymer adsorbent at varied S/L ratio is shown in Fig. 7. Among all prepared samples, only six samples were selected for analysis based on their removal efficiency of having the highest and lowest value from the three different samples used namely MK/S1, MK/S3 and pure MK based geopolymer adsorbents at varied S/L ratio. Upon activation process, the crystalline phases are dissolved in the alkaline solution and the aluminosilicate is formed through geopolymerization reaction. This can be confirmed by observing the reduction in the intensity of the crystalline peaks in synthesized geopolymer in comparison to before geopolymerization. After geopolymerization, a wide diffraction hump in the range between 20 ° to 35 ° in Fig. 7

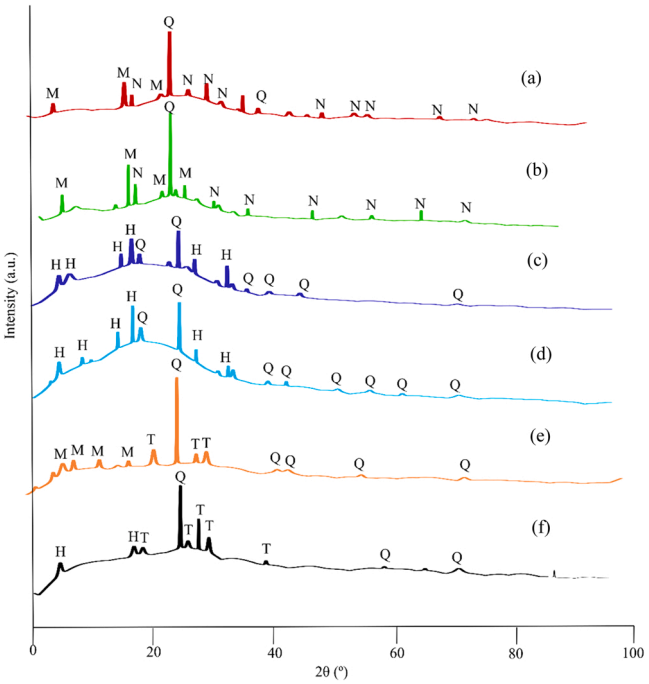

Fig. 7. XRD pattern of synthesized geopolymer adsorbents (Q- quartz (SiO_2), N- nepheline ($2NaAlSiO_4$), T- Anorthite ($CaAl_2Si_2O_8$), H-magnetite (Fe_3O_4), A- albite ($Na(AlSi_3O_8)$, M-muscovite ($KAl_2(AlSi_3O_{10})(OH)$).

(a) and (b) indicates an amorphous structure of MK geopolymer and it is attributed to amorphous aluminosilicate gel which is the primary binder phase in geopolymer. New peaks related to nepheline are formed upon geopolymerization of pure MK at low and high S/L ratio while characteristics of peaks for quartz and muscovite still exist in the range between 5° and 35° as shown in Eq. (2). However, when compared to the raw material, the number of these reflections is lower. On the other hand, synthesized geopolymer adsorbent at 25 % MK and 75 % of S1 at low S/L ratio has formed albite phases as shown in Eq. (3) and less unreacted peaks of quartz and hematite is remained. Whereas, at high S/L ratio, most unreacted peaks correspond to quartz and magnetite as shown in Fig. 7(c)

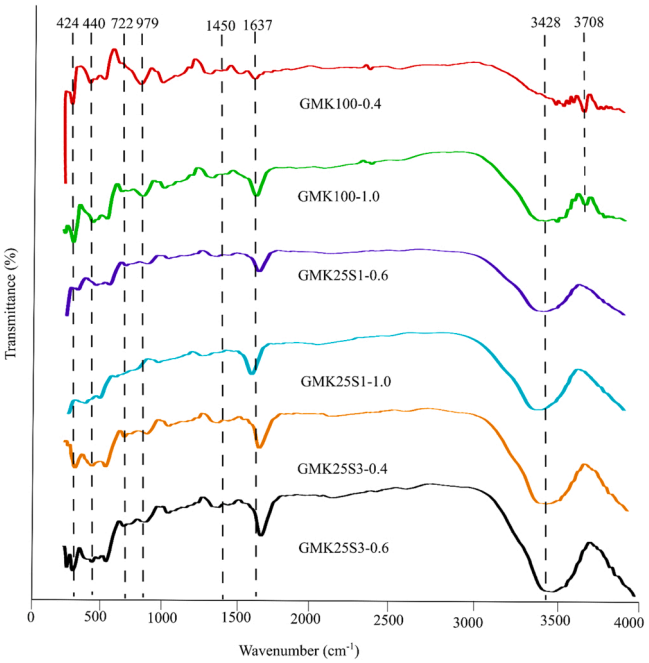

Fig. 8. FTIR spectra of synthesized geopolymer adsorbents.

and (d). This indicates that at high S/L ratio, the aluminosilicate precursors do not dissolve completely due to the lack of alkaline solution. In addition, geopolymer adsorbent containing 25 % of MK and 75 % of S3 synthesized at S/L ratio of 0.6 is well geopolymerized and has formed anorthite phases as shown in Eq. (4). While at S/L ratio of 0.4, these geopolymer adsorbent has formed anorthite and most of the peaks related to quartz and muscovite still remained unreacted due to lack of the interaction between aluminosilicate precursor and excess alkaline solution as shown in Fig. 7(e) and (f).

The halo peak with 2θ between 18 ° and 38 ° for MK is now between 20 ° and 45 ° for geopolymers which is the fingerprint of geopolymerization. However, the amorphous peak in the XRD patterns (Fig. 7(c,d,e,f)) clearly migrated towards 18 ° and 38 ° with S1 and S3 addition in the geopolymer system, demonstrating the unreacted MK at high sludge containing geopolymers [40]. Besides, some of the raw materials' peaks attenuated or disappeared when compared to the synthesized geopolymers, indicating crystalline phase breakdown and geopolymer formation [40]. In addition, the presence of characteristics of quartz in all geopolymer sample suggests that quartz was not involved in the geopolymerization reaction due to low dissolution of quartz in alkaline solution [50]. According to Zibouche et al. [51], the presence of quartz has no effect on the geopolymerization reaction.

$$Na_2O + Al_2O_3 + 2SiO_2 \rightarrow 2NaAlSiO_4 \quad (Nepheline) \tag{2}$$

$$Na_2O + Al_2O_3 + 6SiO_2 \rightarrow 2Na(AlSi_3O_8) \quad (Albite) \tag{3}$$

$$CaO + Al_2O_3 + 2SiO_2 \rightarrow CaAl_2Si_2O_8 (Anorthite) \tag{4}$$

The functional groups of an adsorbent are important to aid in the adsorption process as it provides attachment sites for the adsorbates and then increase the binding capacity with heavy metal ions [52]. The FTIR spectra of synthesized geopolymer at different compositions of MK/S1, MK/S3 and pure MK at varied S: L ratio are illustrated in Fig. 8. The absorption peaks of FTIR located at approximately 3428 cm-^{1} and 1637 cm-^{1} are corresponded to stretching and bending vibration of -OH groups respectively. This broad bands belong to weakly–bound water molecules adsorbed on the surface or trapped between the rings of the geopolymeric products [53]. However, the existence of new peak at about 3708 cm^{-1} in pure MK based geopolymer is assigned to the inner O–H stretching frequency which is bound to the octahedral Al. This might be attributed to the incomplete dihydroxylation of kaolinite. Moreover, the peaks at approximately 1450 cm^{-1} are due to stretching vibration of O-C-O in CO_3^{2-}. Entrapment and dissolution of CO_2 in alkaline activator from atmosphere generate Na_2CO_3 in pure MK and MK/S1 geopolymeric matrix by the reaction of excess NaOH with CO_2 in air [54]. Besides, dissolution of a part of carbonate mineral from sludge in the alkaline activator also generates CO_3^{2-} in the geopolymer matrix of MK/S3.

Besides, there is only a little difference in the FTIR spectra of MK and geopolymers in the range between 4000 cm^{-1} and 400 cm^{-1}. This indicates that the geopolymerization product retains the most vibrant forms of the molecular chains present in the raw material [55]. The displacements in the peak at 747 cm^{-1} in MK which are related to Si-O-Al to lower wavenumber at approximately 722 cm^{-1} after geopolymerization indicates the formation of geopolymeric structure with the transition hexa-to-tetra coordinated Al(IV) [50, 56]. However, in a study by Kaya et al. [40], the major FTIR band of MK at 989 cm^{-1} was observed to be systematically shifted to 1004 cm^{-1}, possibly as a result of more unreacted metakaolin being present in the system with increasing red mud content. This can be slightly correlated with this study at which the band at 979 cm^{-1} in the sample of 0 % of sludge is displaced with the increment of sludge up to 75 %. This indicates the presence of unreacted MK precursor in the GMK25S1 and GMK25S3. In contrast, the bending of the zeolite framework T-O created the bands at approximately 424 cm^{-1} and 440 cm^{-1} due to the transformation of the TO tetrahedral (T = Si, Al, Ca, Mg and etc) [54,57]. The presence of CO_3^{2-} in the geopolymer matrix could promote the adsorption efficiency by the precipitation with Cu^{2+} [58]. In addition, ion complexation of Cu^{2+} with OH^- functional groups could reduce Cu^{2+} in the aqueous solution as shown in Fig. 9. However, Si–O–Si/Al unit does not have an adsorption function, but serves as the adsorbent's skeleton and strengthens the geopolymer adsorbent [59].

The morphology of synthesized geopolymer adsorbent which has been selected based on high removal efficiency of Cu^{2+} is shown in Fig. 10. Fig. 10(a) and (b) show the morphology of pure metakaolin based geopolymer at high and low S: L ratio. The layered like

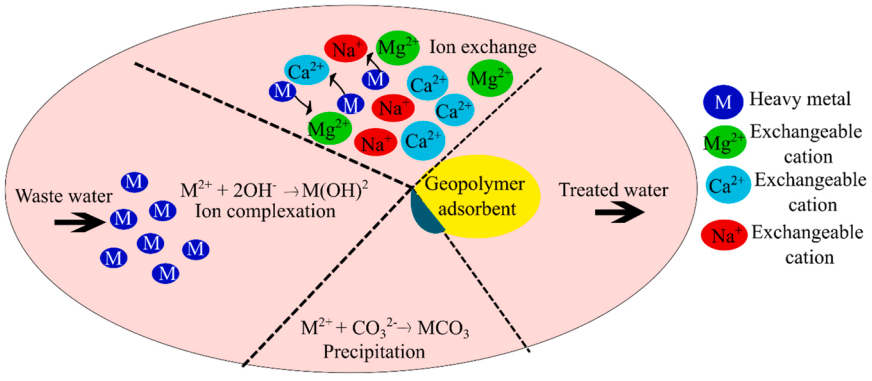

Fig. 9. Adsorption mechanism of synthesized geopolymer adsorbent.

structure of MK almost remained the same after geopolymerization process [55]. While, the surface layer of geopolymer contained S1 sludge is changed from sphere like to sphere like with sharp edges as shown in Fig. 10(c) and (d). This morphological change in MK/S1 based geopolymer is caused by dissolution of aluminosilicate material by alkaline activator especially at low S: L ratio [60]. In contrast, Fig. 10(e) and (f) indicate MK/S3 based geopolymer maintaining the flake like structure of sludge and is a uniformly distributed particles at slightly high S: L ratio. This observation indicates that, alkaline activation only occurs at the outer surface of the raw materials and thus its main shape is maintained since the solid-liquid reaction system provides a gel system [61].

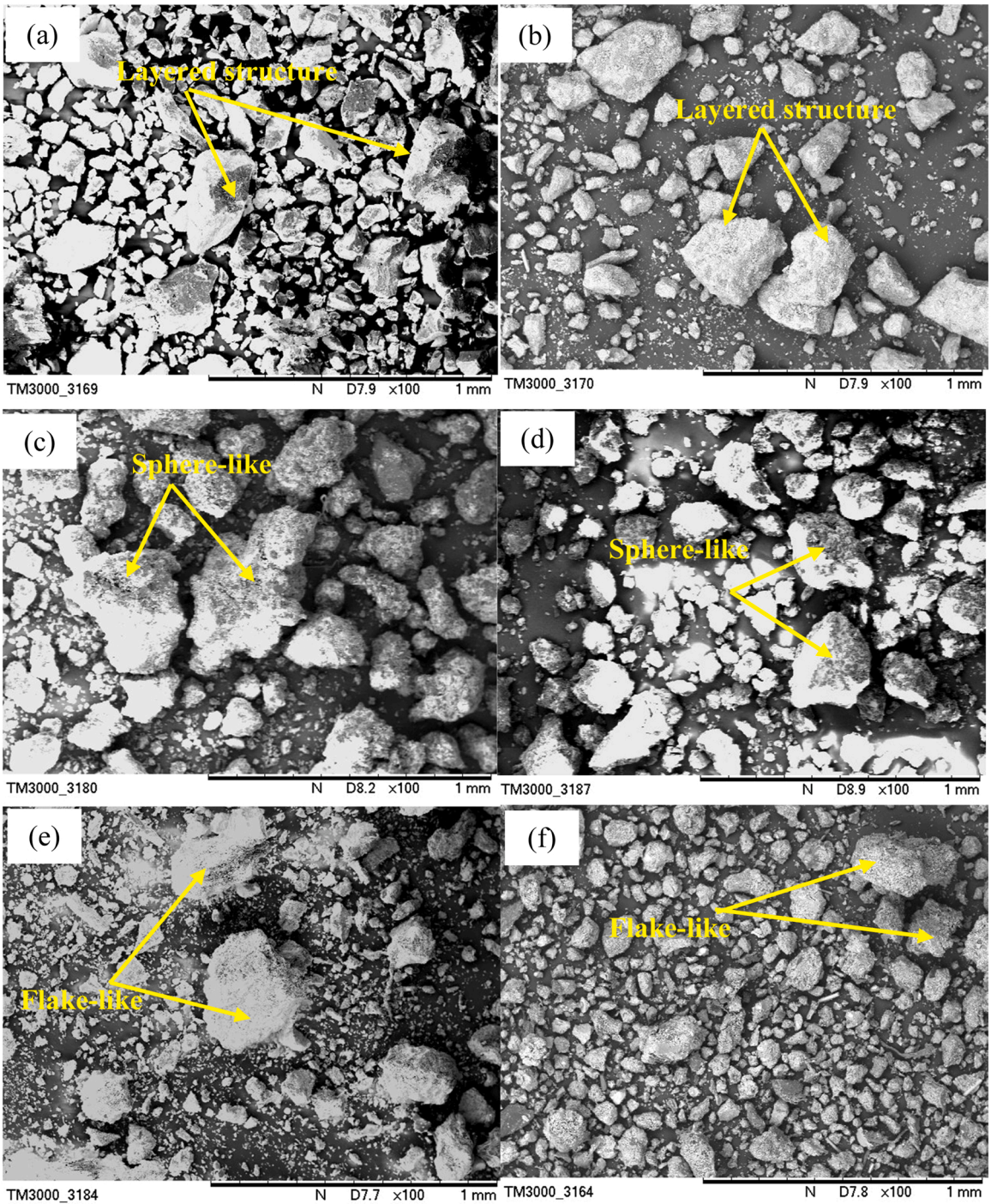

Fig. 10. Morphology of synthesized geopolymer (a) GMK100–0.4, (b) GMK100–1.0, (c) GMK25S1–0.6, (d) GMK25S1–1.0, (e) GMK25S3–0.4 and (d) GMK25S3–0.6.

3.3. Effect of S: L ratio on Cu^{2+} removal efficiency

Fig. 11 shows the Cu^{2+} removal efficiency by MK, S1 and S3 without geopolymerization. Pure MK and S1 yielded similar results of Cu^{2+} removal efficiency at approximately 6.85 % and 5.17 % respectively, while, S1 has achieved the lowest Cu^{2+} removal efficiency. However, the Cu^{2+} removal efficiency by pure S3 is highest (46.31 %) compared to MK and S1 without geopolymerization.

This can contribute to a better chemical and physical properties of S3 compared to MK and S1. S3 has greater amount of MgO, CaO and Fe_2O_3 than MK and S1. Small amount of Cu^{2+} ions get adsorbed by pure S3 adsorbent particles by ion exchange mechanism with Ca and Mg. The ion exchangeability between Cu^{2+} and Ca^{2+} by S3 adsorbent particles is greater than the ion exchangeability between Cu^{2+} and Mg^{2+} in comparison to S1 and MK. This is due to the greater ionic radius of Ca^{2+} (0.100 nm) than Mg^{2+} (0.072 nm) which will be exchanged by Cu^{2+} (0.072 nm) [62]. Apart from that, smaller flake size of S3 adsorbent size particles can adsorb more Cu^{2+} ions faster due to higher surface area which provides more active sites [63]. In contrast, a research by Xu et al. [58] investigated the removal efficiency of Cu, Zn and As by using paper milled sludge derived biochar and found that the removal efficiencies of Cu, Zn, and As were above 95 % due to the wide pores, abundant carbonates, and OH groups.

Fig. 12 shows the Cu^{2+} removal efficiency by 100 % of MK based adsorbent with and without geopolymerization. Pure MK based adsorbent without geopolymerization has the lowest removal efficiency (6.85 %) compared to pure MK based geopolymer adsorbent. Geopolymer adsorbent has obtained the highest Cu^{2+} removal efficiency of approximately 98.56 % at S: L ratio of 0.4. On the other hand, a study conducted by Tunali et al. [64] indicated the high removal efficiency of Cu^{2+} at about 95.02 % by using MK based geopolymer adsorbent. However, this value is lower than the value obtained in this study. Thus, it can be said that, geopolymerization has improved the adsorption capacity of the adsorbent and this might be due to the formation of nepheline phase upon geopolymerization of 100 % of MK [65,66].

The geopolymerization process is conducted at different S: L ratio in which the ratio of aluminosilicate material to alkaline activator varied. The dissolution process and subsequent reaction are influenced by the properties of the solid aluminosilicate, while the liquid activator dissolves the solid raw material partially or entirely, determining aluminosilicate structure break and recombination, polycondensation, and charge balance in the reaction system [33]. Besides, geopolymer synthesized at low S: L ratio is considered at the optimum ratio for better geopolymerization process of pure MK and for improved removal efficiency. This is further explained by the layered structure of MK which limits the mobility of the particles during mixing [67]. Thus, MK based geopolymer requires low S/L ratio to obtain a homogeneous reaction mixture.

The effect of S: L ratio on the Cu^{2+} removal efficiency by MK/S1 and MK/S3 based adsorbent without and with geopolymerization at 75 %, 50 % and 25 % of MK is shown in Fig. 13. The sample with 75 %, 50 % and 25 % of MK without geopolymerization has lower Cu^{2+} removal efficiency compared to sample with geopolymerization. The Cu^{2+} removal efficiency by GMK75S1 fluctuates with increasing S: L ratio from 0.4 to 1.0 as shown in Fig. 13(a). 98.62 % of Cu^{2+} removal efficiency is achieved by GMK75S1–0.4, while this value is decreased to 73.15 % with increasing S: L ratio. However, in comparison to S1, S3 incorporated MK based geopolymer which has low Cu^{2+} removal efficiency at lowest S: L ratio (0.4) is increased by 12.44 % and has attained highest Cu^{2+} removal efficiency of 99.07 % at GMK75S3–0.6. This value further dropped with the increase in S: L ratio and the lowest removal efficiency was obtained at GMK75S3–1.0.

While, the effect of S: L ratio on the removal efficiency by MK/S1 and MK/S3 based geopolymer at 50 % of MK is shown in Fig. 13 (b). Similar trend of Cu^{2+} removal efficiency by MK/S1 and MK/S3 based geopolymer at 75 % of MK is obtained at 50 % of MK. GMK50S1–0.4 with removal efficiency of 98.36 % is reduced by 1.94 % and 15.92 % at S: L ratio of 0.6 and 0.8 respectively followed by an increment at GMK50S1–1.0 to about 84.54 % of removal rate. Whereas, the Cu^{2+} removal efficiency of GMK50S3–0.4 (97.34 %) further raised to 97.55 % at GMK50S3–0.6 before starting to fall to 86.05 % at GMK50S3–1.0. This result indicates that, higher S/L ratio deteriorates the adsorption capacity of MK/S based adsorbents.

In contrast, the relationship between varied S: L ratio and the Cu^{2+} removal efficiency by the prepared geopolymer adsorbents at 25 % of MK is revealed in Fig. 13(c). 75 % of S1 and S3 filled MK based geopolymer adsorbent synthesized at S: L ratio of 0.6 achieved the highest removal efficiency among all compositions at 99.62 % and 99.37 % respectively. In comparison to previous study, the removal efficiency of Cu^{2+} obtained by the fly ash and iron ore tailing based geopolymer incorporated hydrogen peroxide was 90.7 %. Besides, a study by Tan et al. [68] on the removal efficiency of Cu^{2+} by facile fabricated foamed geopolymer sphere found that the removal efficiency increased from 47.5 % to 92.8 % due to the increasing number of binding sites. While, the removal efficiency of

Fig. 11. Removal efficiency by 100 % raw materials.

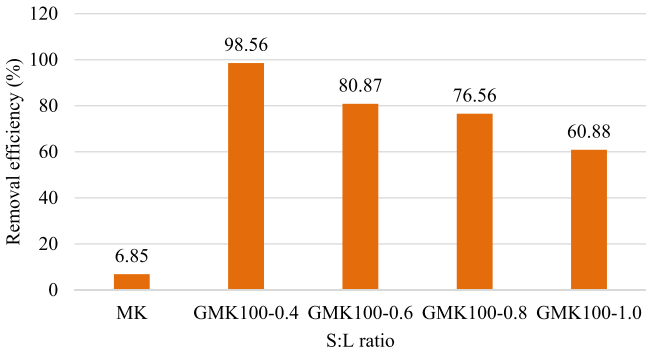

Fig. 12. Removal efficiency by 100 % MK without and with geopolymerization (G).

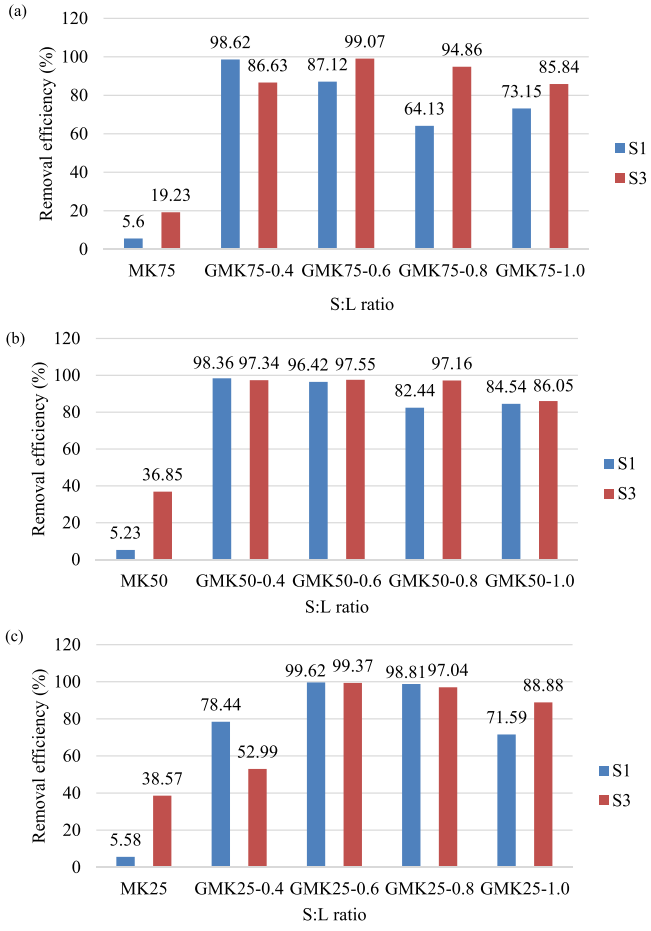

Fig. 13. Removal efficiency by MK/S1 and MK/S3 geopolymer at (a) 75 % of MK, (b) 50 % of MK and (c) 25 % of MK without and with geopolymerization (G).

Cu^{2+} obtained by synthesized adsorbent in this study is greater than previous studies. Thus, geopolymer adsorbents prepared at 25 of MK and 75 % S1 and S3 are considered the best ratios for an effective adsorbent among all compositions. Hence, at this ratio, MK/S based geopolymer synthesized at S: L ratio of 0.6 is chosen as an optimum ratio, whereas pure MK based geopolymer adsorbents prepared at 0.4 is chosen as the best S:L ratio.

This might be due to high water demand of MK compared to S which influences the S/L ratio of the geopolymerization process [69]. Diminished MK content in sample of GMK25S1/S3 will result in the reduction of moisture absorption by MK at S/L ratio of 0.4. Hence, there will be more liquid medium than the solid precursors in the mix which will lead to incomplete reaction between them [34]. However, increasing MK content by increasing S/L ratio at 0.6 improved the reaction between the alkaline activator and the

aluminosilicate materials and enhanced the geopolymerization process. In addition, at higher S/L ratio, the solid precursors do not dissolve properly due to the lack of alkaline solution in the matrix resulting in the inefficient hydrolysis reactions and gel formation [70,71]. This is because, the kinetics of the interchange of silicate units between species during geopolymerization is affected by an increase in the S/L ratio, which results in larger oligomers. This leads to a significant increase in the viscosity of the solution, limiting the workability of the activated pastes as a consequence [72]. In contrast, low S: L ratio hastens the dissolution of MK and promotes polycondensation of geopolymer [48,67,72]. This is due to the presence of sufficient OH^- to catalyze the activation of the precursor by completely dissolving the reactive ions aluminosilicate precursors and Na^+ to balance the charge deficit of aluminum [67]. Besides, MK/S3 based geopolymer has greater removal efficiency even at low concentration with higher removal rate of Cu^{2+} compared to MK/S1. This can be correlated with high specific surface area and average pore size of MK and S3 compared to S1 [73]. Larger surface area offers more active sites for better adsorption performance. Whereas, with the incorporation of high content of sludge into MK, MK/S1 based geopolymer had shown greater Cu^{2+} removal efficiency compared to MK/S3. This can be correlated with the structural changes from sphere like to sphere like with sharp edges which is caused by the greater dissolution of S1 material by alkaline activator. The greater the exposure of S1 towards alkaline activator, the greater the removal efficiency.

3.4. Elemental mapping on the synthesized geopolymer adsorbents

The elemental distribution of Si and Al on pure MK, MK/S1 and MK/S3 geopolymer based adsorbent prepared at low S/L ratio has obtained highest Cu^{2+} removal efficiency compared to pure MK based geopolymer as illustrated in Fig. 14. The color bar indicates the concentration level of elements at which red color represents high concentration and blue color represents low concentration. The distribution of Si and Al allowed for the identification of backbone of the geopolymer (Si-O-Si/Al) [74]. Even distribution of medium concentration of Si region in all three samples can be seen. This emphasizes the homogeneity of the geopolymer samples which is related to nepheline and albite phases. However, only low concentration of Al can be noticed in Fig. 14(a) and (b). Whereas, evenly distributed medium concentration of Al and randomly distributed high concentration of Al in Fig. 14(c) reflect the anorthite phase. This distribution of Al in the geopolymer matrix might lead to greater capacity for Cu^{2+} adsorption.

Fig. 15 reveals the elemental distribution of Si and Al in the sample of pure MK, MK/S1 and MK/S3 based geopolymer adsorbent that has lower Cu^{2+} removal efficiency. Greater distribution of Si and Al is attributed to quartz and muscovite as can be observed in Fig. 15(a) and (b) which was due to the remaining of unreacted phases. However, the distribution of medium concentration and high concentration of Si and Al are more obvious in GMK25S3 at S/L ratio of 0.4 as shown in Fig. 15(c) than the other two samples which represent muscovite and sillimanite phases. This might be due to incomplete geopolymerization reaction between MK/S3 and alkaline activator.

The fundamental structural components of geopolymers are Si and Al, and Si/Al is an important factor to take into account when deciding on a geopolymer application. The ratio of SiO_2/Al_2O_3 which comes from aluminosilicate solid precursors is directly proportional to the setting time of geopolymer. Increase in the alkaline activator delays the reaction of geopolymerization and requires longer coagulation time [75]. This can be further explained by the less contact between alkaline activator and reacting materials as illustrated in Fig. 16(a). There was more fluid medium than solid content in the mix, and the contact between the activating solution and the reacting materials was far and limited. Thus, it was believed that as the alkaline attack began on the material's outer surface, the dissolution of aluminosilicate materials would be slowed down. Besides, precipitation of reactive species occurs with increasing S/L ratio as shown in Fig. 16(c). Increasing S/L ratio increases the amount of aluminosilicate precursors. A small amount of alkaline activator is insufficient to provide an alkaline environment for the MK, S1 and S3 to complete the polymerization reaction and resulting in the inefficient hydrolysis reactions and gel formation. Therefore, most of the phases remain unreacted due to low dissolution of aluminosilicate precursors at low liquid content [71], while geopolymer adsorbent synthesized at optimum S/L ratio results in excellent homogeneity of the sample as revealed in Fig. 16(b).

4. Conclusion

In this study, the best formulation for the synthesis of geopolymer based adsorbent with highest removal efficiency in terms of MK and sludge composition and the optimum S/L ratio was determined. Besides, the characteristics of raw materials and synthesized geopolymer adsorbents were analyzed based on phases present, functional groups and changes in microstructure. Based on the results obtained from the analysis and experimental data, the following conclusions can be derived:

- The optimum ratio of MK to S1 and MK to S3 is 25:75 among all compositions as it has achieved highest Cu^{2+} removal efficiency at approximately 99.62 % and 99.37 % respectively compared to pure MK based geopolymer with 98.56 %. The best S/L ratio for MK/S1 and MK/S3 is 0.6 at which the reaction between the alkaline activator and the aluminosilicate materials has improved and enhanced the geopolymerization process.
- At low S/L ratio, it hastens the dissolution of MK and promotes polycondensation of geopolymer. This is further explained by the layered structure of MK which limits the mobility of the particles during mixing. Thus, MK based geopolymer requires low S/L ratio to obtain a homogeneous reaction mixture. Besides, at low S/L ratio, the presence of sufficient OH^- catalyzes the activation of the precursor by completely dissolving the reactive ions aluminosilicate precursors and Na^+ balances the charge deficit of aluminum.
- However, at higher S/L ratio, it deteriorates the removal efficiency of MK/S1 and MK/S3 based adsorbents. At higher S/L ratio, the solid precursors do not dissolve properly due to the lack of alkaline solution in the matrix resulting in inefficient hydrolysis reactions and gel formation.

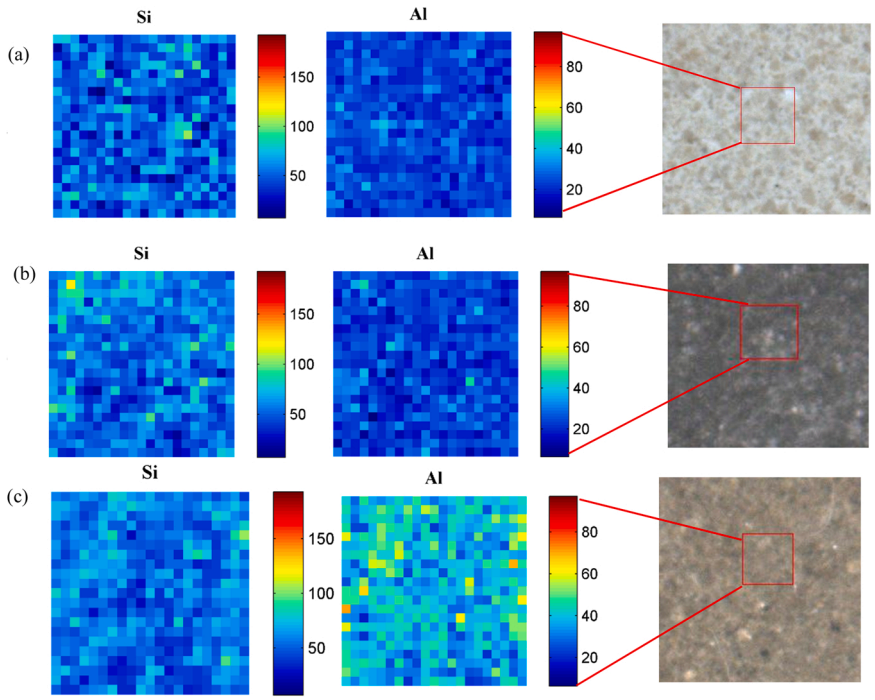

Fig. 14. Elemental mapping of Si and Al (a) GMK100–0.4, (b) GMK25S1–0.6 and (c) GMK25S3–0.6.

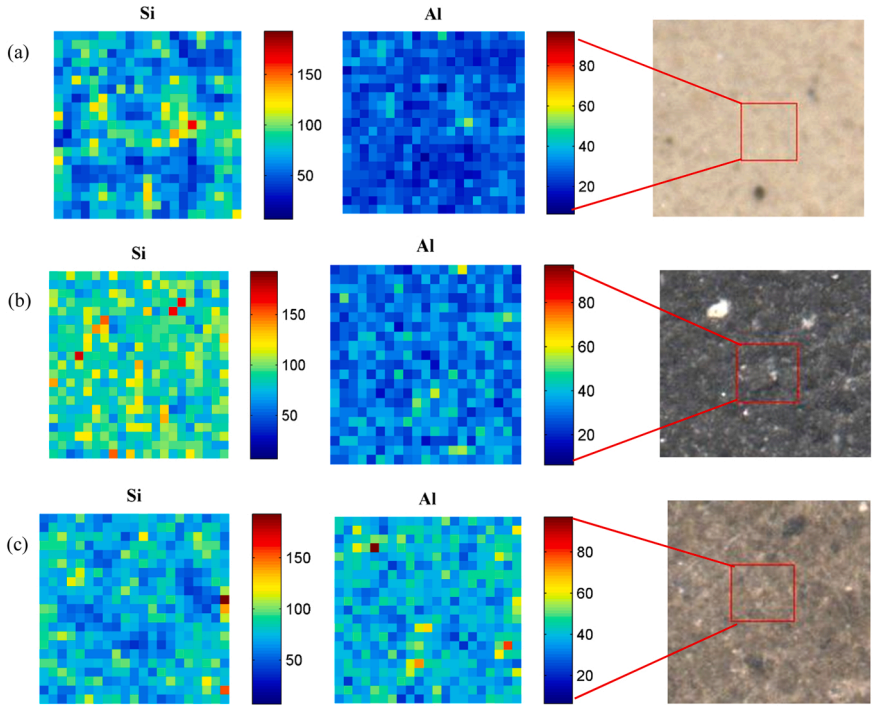

Fig. 15. Elemental mapping of Si and Al (a) GMK100–1.0, (b) GMK25S1–1.0 and (c) GMK25S3–0.4.

- Increase in the alkaline activator delayed the reaction of geopolymerization and required longer coagulation time. This can be further explained by the less contact between alkaline activator and reacting materials. There was more fluid medium than solid content in the mix, and the contact between the activating solution and the reacting materials was far and limited.

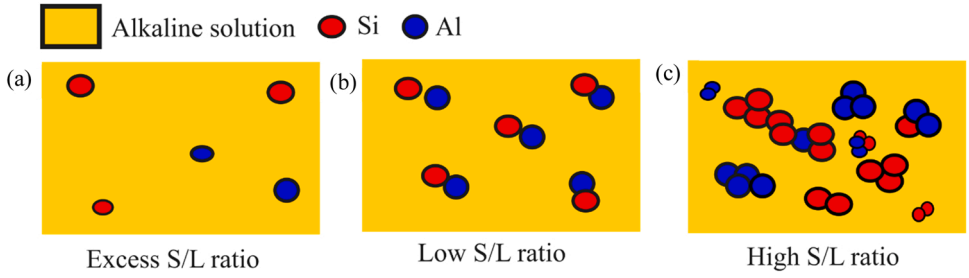

Fig. 16. Schematic diagram of Si/Al distribution at varied S/L ratio.

- The presence of CO_3^{2-} in the geopolymer matrix could promote the adsorption efficiency through the precipitation with Cu^{2+}. In addition, ion complexation of Cu^{2+} with OH^- functional groups could reduce Cu^{2+} in the aqueous solution. Besides, the presence of metal oxide such as CaO and MgO offer ion-exchangeability with Cu^{2+}.

The effectiveness of an adsorbent is influenced by the physical and chemical properties of the adsorbents. An ideal adsorbent material should have a small volume and greater surface area. Apart from that, additional characteristics must include strong mechanical strength, chemical and thermal stability, high porosity and small pore diameter, which result in increased exposed surface area and adequate surface chemistry, leading to high adsorption capacity. Thus, the mechanical properties of the adsorbent are crucial to support the application in wastewater treatment. Therefore, the synthesized metakaolin/sludge geopolymer adsorbent in this study should be further investigated by sintering at various sintering temperature and then subjected to compressive test in order to investigate the compressive strength of the adsorbent before and after heat treatment to be applied in wastewater treatment.

Declaration of Competing Interest

The authors declare that they have no known competing financial interests or personal relationships that could have appeared to influence the work reported in this paper.

Data Availability

No data was used for the research described in the article.

Acknowledgements

The authors gratefully acknowledge the Ministry of Higher Education, Malaysia, through the Fundamental Research Grant Scheme (FRGS) under reference no. FRGS/1/2020/TK0/UNIMAP/01/2 The authors would like to acknowledge Geopolymer and Green Technology, Centre of Excellence (CEGeoGTech), University Malaysia Perlis (UniMAP), Faculty of Chemical Engineering Technology, UniMAP for the support. Special thanks are dedicated to Synchrotron Light Research Institute (SLRI), Thailand for testing and data analyses.

References

[1] Q. Kong, X. Shi, W. Ma, F. Zhang, T. Yu, F. Zhao, D. Zhao, C. Wei, Strategies to improve the adsorption properties of graphene-based adsorbent towards heavy metal ions and their compound pollutants: a review, J. Hazard. Mater. 415 (2021), 125690, https://doi.org/10.1016/j.jhazmat.2021.125690.
[2] W.S. Chai, J.Y. Cheun, P.S. Kumar, M. Mubashir, Z. Majeed, F. Banat, S.H. Ho, P.L. Show, A review on conventional and novel materials towards heavy metal adsorption in wastewater treatment application, J. Clean. Prod. 296 (2021), 126589, https://doi.org/10.1016/j.jclepro.2021.126589.
[3] İ. Kara, D. Yilmazer, S.T. Akar, Metakaolin based geopolymer as an effective adsorbent for adsorption of zinc(II) and nickel(II) ions from aqueous solutions, Appl. Clay Sci. 139 (2017) 54–63, https://doi.org/10.1016/j.clay.2017.01.008.
[4] A. Demirbas, Heavy metal adsorption onto agro-based waste materials: a review, J. Hazard. Mater. 157 (2008) 220–229, https://doi.org/10.1016/j.jhazmat.2008.01.024.
[5] Y. Li, H. Yu, L. Liu, H. Yu, Application of co-pyrolysis biochar for the adsorption and immobilization of heavy metals in contaminated environmental substrates, J. Hazard. Mater. 420 (2021), 126655, https://doi.org/10.1016/j.jhazmat.2021.126655.
[6] S.A. Razzak, M.O. Farooque, Z. Alsheikh, L. Alsheikhmohamad, D. Alkuroud, A. Alfayez, S.M.Z. Hossain, M.M. Hossain, A comprehensive review on conventional and biological-driven heavy metals removal from industrial wastewater, Environ. Adv. 7 (2022), 100168, https://doi.org/10.1016/j.envadv.2022.100168.
[7] F.Y. Aljaberi, Studies of autocatalytic electrocoagulation reactor for lead removal from simulated wastewater, J. Environ. Chem. Eng. 6 (2018) 6069–6078, https://doi.org/10.1016/j.jece.2018.09.032.
[8] M. Jiang, X. Jin, X. Lu, Z. Chen, Adsorption of Pb(II), Cd(II), Ni(II) and Cu(II) onto natural kaolinite clay, Desalination 252 (2010) 33–39, https://doi.org/10.1016/j.desal.2009.11.005.
[9] A.S. Mestre, R.A. Pires, I. Aroso, E.M. Fernandes, M.L. Pinto, R.L. Reis, M.A. Andrade, J. Pires, S.P. Silva, A.P. Carvalho, Activated carbons prepared from industrial pre-treated cork: sustainable adsorbents for pharmaceutical compounds removal, Chem. Eng. J. 253 (2014) 408–417, https://doi.org/10.1016/j.cej.2014.05.051.
[10] S. Babel, T.A. Kurniawan, Low-cost adsorbents for heavy metals uptake from contaminated water: a review, J. Hazard. Mater. 97 (2003) 219–243, https://doi.org/10.1016/S0304-3894(02)00263-7.

[11] I. Chimanlal, M. Lesaoana, H. Richards, Chemical modification of Macadamia -derived activated carbon for remediation of selected heavy metals from wastewater, Miner. Eng. 184 (2022), 107663, https://doi.org/10.1016/j.mineng.2022.107663.
[12] M. Sultana, M.H. Rownok, M. Sabrin, M.H. Rahaman, S.M.N. Alam, A review on experimental chemically modified activated carbon to enhance dye and heavy metals adsorption, Clean. Eng. Technol. 6 (2022), 100382, https://doi.org/10.1016/j.clet.2021.100382.
[13] M. Mariana, A.K. Abdul, E.M. Mistar, E.B. Yahya, T. Alfatah, M. Danish, M. Amayreh, Recent advances in activated carbon modification techniques for enhanced heavy metal adsorption, J. Water Process Eng. 43 (2021), 102221, https://doi.org/10.1016/j.jwpe.2021.102221.
[14] P.N. Das, K. Jithesh, K.G. Raj, Recent developments in the adsorptive removal of heavy metal ions using metal-organic frameworks and graphene-based adsorbents, J. Indian Chem. Soc. 98 (2021), 100188, https://doi.org/10.1016/j.jics.2021.100188.
[15] M.N. Mužek, S. Svilović, J. Zelić, Fly ash-based geopolymeric adsorbent for copper ion removal from wastewater, Desalin. Water Treat. 52 (2014) 2519–2526, https://doi.org/10.1080/19443994.2013.792015.
[16] I. Luhar, S. Luhar, M.M.A.B. Abdullah, R.A. Razak, P. Vizureanu, A.V. Sandu, P.-D. Matasaru, A state-of-the-art review on innovative geopolymer composites designed for water and wastewater treatment, Mater. (Basel) 14 (2021) 7456, https://doi.org/10.3390/ma14237456.
[17] A.A. Siyal, M.R. Shamsuddin, M.I. Khan, N.E. Rabat, M. Zulfiqar, Z. Man, J. Siame, K.A. Azizli, A review on geopolymers as emerging materials for the adsorption of heavy metals and dyes, J. Environ. Manag. 224 (2018) 327–339, https://doi.org/10.1016/j.jenvman.2018.07.046.
[18] P. He, Y. Zhang, X. Zhang, H. Chen, Diverse zeolites derived from a circulating fluidized bed fly ash based geopolymer for the adsorption of lead ions from wastewater, J. Clean. Prod. 312 (2021), 127769, https://doi.org/10.1016/j.jclepro.2021.127769.
[19] S. Hu, L. Zhong, X. Yang, H. Bai, B. Ren, Y. Zhao, W. Zhang, X. Ju, H. Wen, S. Mao, R. Tao, C. Li, Synthesis of rare earth tailing-based geopolymer for efficiently immobilizing heavy metals, Constr. Build. Mater. 254 (2020), 119273, https://doi.org/10.1016/j.conbuildmat.2020.119273.
[20] X. Chen, Y. Guo, S. Ding, H.Y. Zhang, F.Y. Xia, J. Wang, M. Zhou, Utilization of red mud in geopolymer-based pervious concrete with function of adsorption of heavy metal ions, J. Clean. Prod. (2019), https://doi.org/10.1016/j.jclepro.2018.09.263.
[21] M.T. Marvila, A.R.G. de Azevedo, L.B. de Oliveira, G. de Castro Xavier, C.M.F. Vieira, Mechanical, physical and durability properties of activated alkali cement based on blast furnace slag as a function of %Na2O, Case Stud. Constr. Mater. 15 (2021), e00723, https://doi.org/10.1016/j.cscm.2021.e00723.
[22] L.B. de Oliveira, A.R.G. de Azevedo, M.T. Marvila, E.C. Pereira, R. Fediuk, C.M.F. Vieira, Durability of geopolymers with industrial waste, Case Stud. Constr. Mater. 16 (2022), e00839, https://doi.org/10.1016/j.cscm.2021.e00839.
[23] M.T. Marvila, A.R.G. De Azevedo, P.R. De Matos, S.N. Monteiro, C.M.F. Vieira, Materials for production of high and ultra-high performance concrete: Review and perspective of possible novel materials, Mater. (Basel) 14 (2021), https://doi.org/10.3390/ma14154304.
[24] L. Darmayanti, G.T.M. Kadja, S. Notodarmojo, E. Damanhuri, R.R. Mukti, Structural alteration within fly ash-based geopolymers governing the adsorption of Cu2+ from aqueous environment: effect of alkali activation, J. Hazard. Mater. 377 (2019) 305–314, https://doi.org/10.1016/j.jhazmat.2019.05.086.
[25] L. Panda, S.S. Rath, D.S. Rao, B.B. Nayak, B. Das, P.K. Misra, Thorough understanding of the kinetics and mechanism of heavy metal adsorption onto a pyrophyllite mine waste based geopolymer, J. Mol. Liq. 263 (2018) 428–441, https://doi.org/10.1016/j.molliq.2018.05.016.
[26] Y. Chen, R. Wang, X. Duan, S. Wang, N. Ren, S. Ho, Production, properties, and catalytic applications of sludge derived biochar for environmental remediation, Water Res 187 (2020), 116390, https://doi.org/10.1016/j.watres.2020.116390.
[27] X. Niu, Y. Elakneswaran, C.R. Islam, J.L. Provis, T. Sato, Adsorption behaviour of simulant radionuclide cations and anions in metakaolin-based geopolymer, J. Hazard. Mater. 429 (2022), 128373, https://doi.org/10.1016/j.jhazmat.2022.128373.
[28] G.Z.B. Santos, J.A. Melo, M. Pinheiro, L. Manzato, Synthesis of water treatment sludge ash-based geopolymers in an Amazonian context, J. Environ. Manag. 249 (2019), 109328, https://doi.org/10.1016/j.jenvman.2019.109328.
[29] H. Isa, The need for waste management in the glass industries: A review, 3 (2008) 276–279.
[30] P. Perumal, A. Hasnain, T. Luukkonen, P. Kinnunen, M. Illikainen, Role of surfactants on the synthesis of impure kaolin-based alkali-activated, low-temperature porous ceramics, Open Ceram. 6 (2021), 100097, https://doi.org/10.1016/j.oceram.2021.100097.
[31] H. Wang, C. Li, Z. Peng, S. Zhang, Characterization and thermal behavior of kaolin, J. Therm. Anal. Calor. 105 (2011) 157–160, https://doi.org/10.1007/s10973-011-1385-0.
[32] M. Oualit, A. Irekti, Mechanical performance of metakaolin-based geopolymer mortar blended with multi-walled carbon nanotubes, Ceram. Int. 48 (2022) 16188–16195, https://doi.org/10.1016/j.ceramint.2022.02.166.
[33] C. Zhang, M. Wei, Z. Hu, T. Yang, B. Jiao, H. Zhu, S. Nmr, Sulphate resistance of silane coupling agent reinforced metakaolin geopolymer composites, Ceram. Int (2022), https://doi.org/10.1016/j.ceramint.2022.05.190.
[34] C.Y. Heah, H. Kamarudin, A.M.M. Al, M. Bnhussain, M. Luqman, I.K. Nizar, C.M. Ruzaidi, Y.M. Liew, Study on solids-to-liquid and alkaline activator ratios on kaolin-based geopolymers, Constr. Bulid. Mater. 35 (2012) 912–922, https://doi.org/10.1016/j.conbuildmat.2012.04.102.
[35] S. Alonso, A. Palomo, Alkaline activation of metakaolin and calcium hydroxide mixtures: influence of temperature, activator concentration and solids ratio, Mater. Lett. 47 (2001) 55–62, https://doi.org/10.1016/S0167-577X(00)00212-3.
[36] T. Xie, P. Visintin, X. Zhao, R. Gravina, Mix design and mechanical properties of geopolymer and alkali activated concrete: Review of the state-of-the-art and the development of a new unified approach, Constr. Build. Mater. 256 (2020), 119380, https://doi.org/10.1016/j.conbuildmat.2020.119380.
[37] T.H. Tan, K.H. Mo, T.C. Ling, S.H. Lai, Current development of geopolymer as alternative adsorbent for heavy metal removal, Environ. Technol. Innov. 18 (2020), 100684, https://doi.org/10.1016/j.eti.2020.100684.
[38] O. Ayeni, A.P. Onwualu, E. Boakye, Characterization and mechanical performance of metakaolin-based geopolymer for sustainable building applications, Constr. Build. Mater. 272 (2021), https://doi.org/10.1016/j.conbuildmat.2020.121938.
[39] M. Karatas, A. Benli, F. Arslan, The effects of kaolin and calcined kaolin on the durability and mechanical properties of self-compacting mortars subjected to high temperatures, Constr. Build. Mater. 265 (2020), 120300, https://doi.org/10.1016/j.conbuildmat.2020.120300.
[40] K. Kaya, S. Soyer-uzun, Evolution of structural characteristics and compressive strength in red mud – metakaolin based geopolymer systems, Ceram. Int. 42 (2016) 7406–7413, https://doi.org/10.1016/j.ceramint.2016.01.144.
[41] T. Luukkonen, M. Sarkkinen, K. Kemppainen, J. Rämö, U. Lassi, Metakaolin geopolymer characterization and application for ammonium removal from model solutions and landfill leachate, Appl. Clay Sci. 119 (2016) 266–276, https://doi.org/10.1016/j.clay.2015.10.027.
[42] G.C. Girondi Delaqua, M. das N. Ferreira, L.F. Amaral, R.J. Sánchez Rodríguez, E. Atem de Carvalho, C.M. Fontes Vieira, Incorporation of sludge from effluent treatment plant of an industrial laundry into heavy clay ceramics, J. Build. Eng. 47 (2022), 103451, https://doi.org/10.1016/j.jobe.2021.103451.
[43] Q. Wan, F. Rao, S. Song, D.F. Cholico-González, N.L. Ortiz, Combination formation in the reinforcement of metakaolin geopolymers with quartz sand, Cem. Concr. Compos. 80 (2017) 115–122, https://doi.org/10.1016/j.cemconcomp.2017.03.005.
[44] I.C. Ferreira, R. Galéry, A.B. Henriques, A. Paula de Carvalho Teixeira, C.D. Prates, A.S. Lima, I.R. Souza Filho, Reuse of iron ore tailings for production of metakaolin-based geopolymers, J. Mater. Res. Technol. 18 (2022) 4194–4200, https://doi.org/10.1016/j.jmrt.2022.03.192.
[45] N.H. Jamil, M.M. Al Bakri Abdullah, F.C. Pa, H. Mohamad, W.M.A.W. Ibrahim, J. Chaiprapa, Influences of SiO2, Al2O3, CaO and MgO in phase transformation of sintered kaolin-ground granulated blast furnace slag geopolymer, J. Mater. Res. Technol. 9 (2020) 14922–14932, https://doi.org/10.1016/j.jmrt.2020.10.045.
[46] R. Dewi, H. Agusnar, Z. Alfian, Tamrin, Characterization of technical kaolin using XRF, SEM, XRD, FTIR and its potentials as industrial raw materials, J. Phys. Conf. Ser. 1116 (2018), https://doi.org/10.1088/1742-6596/1116/4/042010.
[47] M. El Alouani, S. Alehyen, M. El Achouri, M. Taibi, Preparation, characterization, and application of metakaolin-based geopolymer for removal of methylene blue from aqueous solution, J. Chem. (2019) 1–14.
[48] Z. Yunsheng, S. Wei, L. Zongjin, Applied clay science composition design and microstructural characterization of calcined kaolin-based geopolymer cement, Appl. Clay Sci. 47 (2010) 271–275, https://doi.org/10.1016/j.clay.2009.11.002.
[49] T. Lan, P. Li, F.U. Rehman, X. Li, W. Yang, S. Guo, Efficient adsorption of Cd2+ from aqueous solution using metakaolin geopolymers, Environ. Sci. Pollut. Res. 26 (2019) 33555–33567, https://doi.org/10.1007/s11356-019-06362-w.

[50] L. Chen, Z. Wang, Y. Wang, J. Feng, Preparation and properties of alkali activated metakaolin-based geopolymer, Mater. (Basel) 9 (2016) 1–12, https://doi.org/10.3390/ma9090767.
[51] F. Zibouche, H. Kerdjoudj, J. Espinose, D. Lacaillerie, H. Van Damme, Applied clay science geopolymers from Algerian metakaolin. in fluence of secondary minerals, Appl. Clay Sci. 43 (2009) 453–458, https://doi.org/10.1016/j.clay.2008.11.001.
[52] A.A. Aryee, F.M. Mpatani, A.N. Kani, E. Dovi, R. Han, Z. Li, L. Qu, A review on functionalized adsorbents based on peanut husk for the sequestration of pollutants in wastewater: modification methods and adsorption study, J. Clean. Prod. 310 (2021), 127502, https://doi.org/10.1016/j.jclepro.2021.127502.
[53] A. Sičáková, N. Števulová, Basic physical – mechanical properties of geopolymers depending on the content of ground fly ash and fines of sludge, Sel. Sci. Pap. - J. Civ. Eng. 12 (2017) 85–96, https://doi.org/10.1515/sspjce-2017-0009.
[54] E. Wei, K. Wang, Y. Muhammad, S. Chen, D. Dong, Y. Wei, T. Fujita, Preparation and conversion mechanism of different geopolymer-based zeolite microspheres and their adsorption properties for Pb2, Sep. Purif. Technol. 282 (2022), 119971, https://doi.org/10.1016/j.seppur.2021.119971.
[55] H. Wang, H. Li, F. Yan, Synthesis and mechanical properties of metakaolinite-based geopolymer, Colloids Surf. A Physicochem. Eng. Asp. 268 (2005) 1–6, https://doi.org/10.1016/j.colsurfa.2005.01.016.
[56] M. El Alouani, H. Saufi, G. Moutaoukil, S. Alehyen, B. Nematollahi, W. Belmaghraoui, M. Taibi, Application of geopolymers for treatment of water contaminated with organic and inorganic pollutants: state-of-the-art review, J. Environ. Chem. Eng. 9 (2021), 105095, https://doi.org/10.1016/j.jece.2021.105095.
[57] W.K. Cai, J.H. Liu, C.H. Zhou, J. Keeling, U.A. Glasmacher, Structure, genesis and resources efficiency of dolomite: new insights and remaining enigmas, Chem. Geol. 573 (2021), https://doi.org/10.1016/j.chemgeo.2021.120191.
[58] Z. Xu, Y. Lin, Y. Lin, D. Yang, H. Zheng, Environmental Technology & Innovation Adsorption behaviors of paper mill sludge biochar to remove Cu, Zn and As in wastewater, Environ. Technol. Innov. 23 (2021), 101616, https://doi.org/10.1016/j.eti.2021.101616.
[59] Q. Su, S. Li, M. Chen, X. Cui, Highly efficient Cd(II) removal using macromolecular dithiocarbamate/slag-based geopolymer composite microspheres (SGM-MDTC), Sep. Purif. Technol. 286 (2022), 120395, https://doi.org/10.1016/j.seppur.2021.120395.
[60] M. El Alouani, S. Alehyen, M. El Achouri, M. Taibi, Preparation, characterization, and application of metakaolin-based geopolymer for removal of methylene blue from aqueous solution, J. Chem. 2019 (2019), https://doi.org/10.1155/2019/4212901.
[61] T.W. Cheng, M.L. Lee, M.S. Ko, T.H. Ueng, S.F. Yang, The heavy metal adsorption characteristics on metakaolin-based geopolymer, Appl. Clay Sci. 56 (2012) 90–96, https://doi.org/10.1016/j.clay.2011.11.027.
[62] E. Pehlivan, A.M. Özkan, S. Dinç, Ş. Parlayici, Adsorption of Cu2+and Pb2+ion on dolomite powder, J. Hazard. Mater. 167 (2009) 1044–1049, https://doi.org/10.1016/j.jhazmat.2009.01.096.
[63] S.P. Lee, G.A.M. Ali, H. Algarni, K.F. Chong, Flake size-dependent adsorption of graphene oxide aerogel, J. Mol. Liq. 277 (2019) 175–180, https://doi.org/10.1016/j.molliq.2018.12.097.
[64] S. Tunali, H. Çolo, F. Sayin, I. Kara, T. Akar, Parametric optimization of Cu (II) removal process by a metakaolin-based geopolymer: Batch and continuous process design, J. Clean. Prod. 366 (2022), 132819, https://doi.org/10.1016/j.jclepro.2022.132819.
[65] Y. Kobayashi, F. Ogata, T. Nakamura, N. Kawasaki, Synthesis of novel zeolites produced from fly ash by hydrothermal treatment in alkaline solution and its evaluation as an adsorbent for heavy metal removal, J. Environ. Chem. Eng. 8 (2020) 3–4, https://doi.org/10.1016/j.jece.2020.103687.
[66] H.S. Gökçe, M. Tuyan, M.L. Nehdi, Alkali-activated and geopolymer materials developed using innovative manufacturing techniques: a critical review, Constr. Build. Mater. 303 (2021), https://doi.org/10.1016/j.conbuildmat.2021.124483.
[67] D. Mulugeta, Z. Liao, U. Berardi, H. Doan, Salient parameters affecting the performance of foamed geopolymers as sustainable insulating materials, Constr. Build. Mater. 313 (2021), 125400, https://doi.org/10.1016/j.conbuildmat.2021.125400.
[68] T.H. Tan, K.H. Mo, S.H. Lai, T.C. Ling, Investigation on the copper ion removal potential of a facile-fabricated foamed geopolymer sphere for wastewater remediation, Clean. Mater. 4 (2022), 100088, https://doi.org/10.1016/j.clema.2022.100088.
[69] D.L.Y. Kong, J.G. Sanjayan, K. Sagoe-Crentsil, Comparative performance of geopolymers made with metakaolin and fly ash after exposure to elevated temperatures, Cem. Concr. Res. 37 (2007) 1583–1589, https://doi.org/10.1016/j.cemconres.2007.08.021.
[70] S. Samantasinghar, S.P. Singh, Effect of synthesis parameters on compressive strength of fly ash-slag blended geopolymer, Constr. Build. Mater. 170 (2018) 225–234, https://doi.org/10.1016/j.conbuildmat.2018.03.026.
[71] P. Duxson, J.L. Provis, G.C. Lukey, S.W. Mallicoat, W.M. Kriven, J.S.J. Van Deventer, Understanding the relationship between geopolymer composition, microstructure and mechanical properties, Colloids Surf. A Physicochem. Eng. Asp. 269 (2005) 47–58, https://doi.org/10.1016/j.colsurfa.2005.06.060.
[72] H. Cheng, K.L. Lin, R. Cui, C.L. Hwang, T.W. Cheng, Y.M. Chang, Effect of solid-to-liquid ratios on the properties of waste catalyst-metakaolin based geopolymers, Constr. Build. Mater. 88 (2015) 74–83, https://doi.org/10.1016/j.conbuildmat.2015.01.005.
[73] C. Wang, Z. Yang, W. Song, Y. Zhong, M. Sun, T. Gan, B. Bao, Quantifying gel properties of industrial waste-based geopolymers and their application in Pb2+ and Cu2+ removal, J. Clean. Prod. 315 (2021), 128203, https://doi.org/10.1016/j.jclepro.2021.128203.
[74] I.H. Aziz, M.M.A.B. Abdullah, M.A.A. Mohd Salleh, E.A. Azimi, J. Chaiprapa, A.V. Sandu, Strength development of solely ground granulated blast furnace slag geopolymers, Constr. Build. Mater. 250 (2020), 118720, https://doi.org/10.1016/j.conbuildmat.2020.118720.
[75] F. Bowen, L. Jiesheng, W. Jing, C. Yaohua, Z. Tongtong, Case studies in construction materials investigation on the impact of different activator to solid ratio on properties and micro-structure of metakaolin geopolymer, Case Stud. Constr. Mater. 16 (2022), e01127, https://doi.org/10.1016/j.cscm.2022.e01127.